

Cite this: *Catal. Sci. Technol.*, 2024,
14, 2178

Mitigated ammonium nitrate inhibition in SCR over Cu-SSZ-13 + Ce/Mn-oxide composite catalysts: insights from temperature-programmed desorption analysis†

Tahrizi Andana,^{‡a} Kenneth G. Rappé, ^{‡*a} Feng Gao^b and Yong Wang^{ac}

This work reports synergistic effects within SCR (selective catalytic reduction) composite catalysts, consisting of Ce/Mn-oxide and Cu-SSZ-13. These effects reduce NH_4NO_3 inhibition on the NO_x -SCR reaction rate at low temperatures in NO_2 -rich environments (e.g., “fast” SCR, $\text{NO}_2/\text{NO}_x = 0.5$). Catalytic performance and kinetics indicate strong influence of Ce/Mn-oxide on both the quantity and nature of NH_4NO_3 deposits. Temperature-programmed desorption/decomposition analyses of NH_4NO_3 -laden composite catalysts, through *in situ* (via pre-exposure to “fast” SCR atmosphere) and *ex situ* (via physical mixture with NH_4NO_3 solid) deposition techniques, reveal (i) reduced deposits formed on the composite catalysts at low temperatures, and (ii) comparatively facile NH_4NO_3 decomposition on the composite catalysts pre-exposed to fast-SCR that is remarkably similar to physically mixed NH_4NO_3 solids. This suggests that during the catalytic fast SCR reaction over the composite catalyst, lower buildup of NH_4NO_3 occurs in the zeolite phase and is deposited in a form that is less stable in the zeolite (i.e., ‘destabilized’). Both observations are believed to be the result of influence by nitrite intermediates generated by Ce/Mn-oxide, the same species responsible for the synergistic effect in standard SCR (i.e., absence of NO_2), and confirm the close contact requirement for the synergistic effects of Ce/Mn-oxide on Cu-SSZ-13. This is, to our knowledge, the first reported effect of SCR composite catalysts reducing the quantity and altering the nature of NH_4NO_3 deposits formed during the SCR reaction at low temperature, and a key step in the design of SCR catalysts with low N_2O evolution and greenhouse gas impact.

Received 15th January 2024,
Accepted 4th March 2024

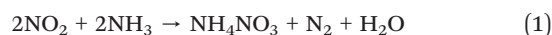
DOI: 10.1039/d4cy00062e

rsc.li/catalysis

Introduction

To meet the target of 90% pollutant reduction at 150 °C from lean burn exhaust mixtures (i.e., “The 150 °C Challenge”),¹ progressive efforts have been made to improve the low-temperature efficiency of existing abatement technologies. For NO_x abatement via selective catalytic reduction by ammonia (NH_3 -SCR), current approaches employ Cu-/Fe-exchanged zeolites as state-of-the-art. However, NO is the primary NO_x species emitted from the engine and the standard SCR reaction ($4\text{NO} + 4\text{NH}_3 + \text{O}_2 \rightarrow 4\text{N}_2 + 6\text{H}_2\text{O}$) is

unable to meet this target.^{2,3} Improved low-temperature efficiency is achievable through the fast SCR reaction ($\text{NO} + \text{NO}_2 + 2\text{NH}_3 \rightarrow 2\text{N}_2 + 3\text{H}_2\text{O}$), particularly over metal-exchanged medium-/large-pore zeolites as well as V-based catalysts.^{4–12} However, carrying out the fast SCR reaction at low temperatures is challenged by temporary deactivation by solid NH_4NO_3 deposits formed via a reaction between NO_2 and NH_3 :^{12–14}



The adverse impact of NH_4NO_3 deactivation does not subside until the exhaust temperature surpasses the NH_4NO_3 melting point (170–180 °C). Above this temperature, solid NH_4NO_3 undergoes: (1) sublimation to gas-phase NH_4NO_3 (eqn (2)),¹⁵ (2) dissociation to NH_3 and HNO_3 (eqn (3)),^{13,15,16} (3) thermal decomposition to NO_x (eqn (4)–(6)),^{16–18} and/or catalytic reduction by NO (eqn (7)).^{19,20} In current aftertreatment systems where the average exhaust temperature is higher than the NH_4NO_3 melting point, the NH_4NO_3 -induced deactivation is temporary and occurs only during “cold-start”.

^a Energy & Environment Directorate, Pacific Northwest National Laboratory, Richland, WA 99354, USA. E-mail: tahrizi.andana@cummins.com, ken.rappe@pnnl.gov

^b Physical & Computational Sciences Directorate, Pacific Northwest National Laboratory, Richland, WA 99354, USA. E-mail: feng_fgao@tju.edu.cn

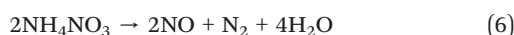
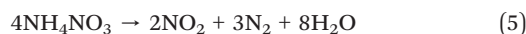
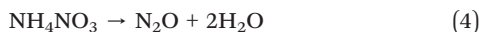
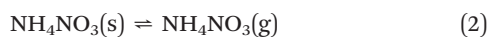
^c The Gene and Linda Voiland School of Chemical Engineering and Bioengineering, Washington State University, Pullman, WA, USA

† Electronic supplementary information (ESI) available. See DOI: <https://doi.org/10.1039/d4cy00062e>

‡ These authors contributed equally to this work.



However, in the abatement systems including hybrid vehicle application, the exhaust temperature can be persistently low. Thus, deactivation from NH_4NO_3 deposits becomes more persistent and sustained NO_x abatement at low temperatures is unachievable.



For metal-exchanged zeolite catalysts, zeolite physicochemical properties identified as key factors in resistance against NH_4NO_3 deactivation include (i) zeolite acidity, (ii) zeolite structure/porosity^{9,17,20–26} and (iii) chemistry of Lewis acid sites.^{2,8,27,28} Zeolite acidity, regardless of strength (*i.e.*, Lewis or Brønsted), has been demonstrated as a key factor in dictating formation and decomposition of NH_4NO_3 during the SCR reaction.^{25,29–31} Zeolite structure and pore size are also important factors. Larger-pore zeolites such as BEA and ZSM-5 generally confer better resistance towards NH_4NO_3 inhibition than small-pore zeolites like CHA, likely due to the exceptional stability of NH_4NO_3 deposit within the confines of the CHA cage.^{17,20,21,23–26} Finally, there is a consistent trend among Cu and Fe metal-exchanged zeolite catalysts concerning their susceptibility to deactivation caused by NH_4NO_3 deposits. Specifically, Cu-zeolites tend to be less active than Fe-zeolites for the low-temperature fast SCR reaction.^{2,8,27,28} This is likely due to a lower affinity of NH_3 toward Fe ions *versus* Cu which potentially underlies their relative tendencies towards NH_4NO_3 inhibition.

We recently demonstrated that combining a metal oxide (*e.g.*, ceria-manganese oxide, $\text{Ce}_{1-x}\text{Mn}_x\text{O}_y$), termed the selective catalytic oxidation (SCO) phase, with Cu-SSZ-13, referred to as the SCR phase, yielded an SCO-SCR composite catalyst with improved SCR performance and reduced NH_4NO_3 inhibition.³² The latter was evidenced by NO_2 evolution from the composite catalysts under low-temperature fast SCR conditions that differed distinctly from Cu-SSZ-13 (Fig. 1A). Particularly, NO_2 consumption accelerates above $\sim 175^\circ\text{C}$ over the impregnated and ball-milled composite catalysts, indicating that NH_4NO_3 decomposition is facilitated over the composite catalysts at reduced temperature *versus* Cu-SSZ-13. Additionally, it was observed that the fast SCR apparent activation energy (E_a) over the impregnated composite catalyst was considerably lower than pure Cu-SSZ-13 and the ball-milled composite catalyst (Fig. 1B). Combined with significantly reduced NO_2 evolution from the impregnated composite catalyst *versus* the ball-milled composite and Cu-

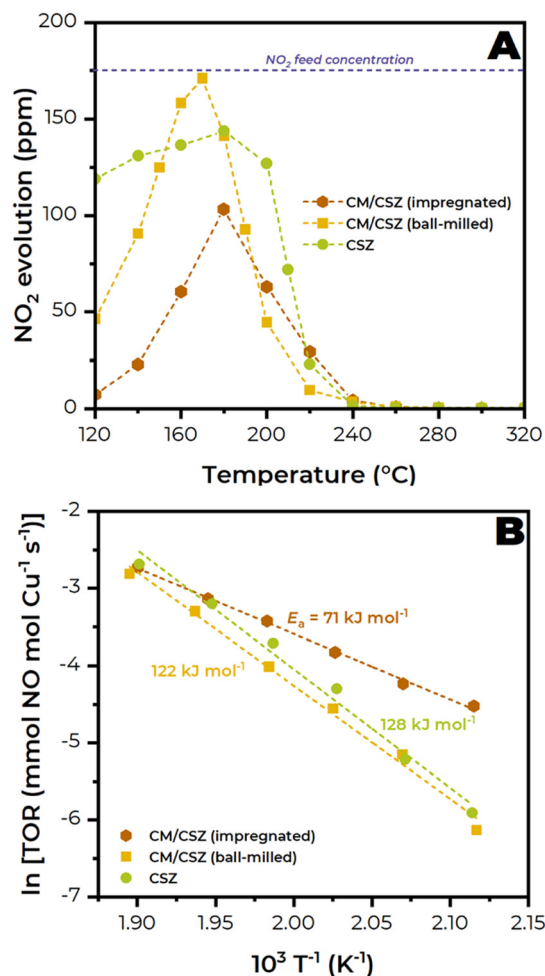


Fig. 1 NO_2 evolution (A, top) and apparent activation energy analysis (B, bottom) under fast SCR reaction conditions with Cu-SSZ-13 (CSZ) and ceria-manganese oxide + Cu-SSZ-13 composite catalysts (CM/CSZ) prepared by impregnation and ball-milling. See [Experimental – “Fast” SCR kinetics] for testing conditions.

SSZ-13 catalysts, this indicates a lower energetic requirement for eqn (7), apparently dependent on the contact intimacy between SCO and SCR, as rate-determining in the “fast” SCR reaction over the composite catalysts.²⁰

Although the advantageous impact of the oxide component is evident, the mechanism through which this promotion occurs remains unclear. In our previous work, we initially ascribed the synergistic effect between SCO and SCR under standard SCR conditions (*i.e.*, absence of NO_2) to the generation of reactive nitrite and nitrite-like active intermediates from the oxide component which are responsible for a synergistic low-temperature SCR reaction.³² However, what is still unclear is the overall performance and kinetic trends under “fast” SCR conditions (Fig. 1) that seem to point to the persistent NH_4NO_3 intermediacy and NH_4NO_3 reduction to NO_2 being a crucial reaction step in the reaction. Since Fig. 1 suggests that NH_4NO_3 still accumulates at low temperatures and remains as a reaction intermediate despite the presence of metal oxide, a question then arises as to how



reduction of NH_4NO_3 exactly occurs and how the oxide component facilitates that process. At reaction temperatures of 160 °C and 170 °C, it is important to note that NO_2 outlet concentrations over the ball-milled composite catalyst are higher than those over the SCR phase alone (Fig. 1A). This phenomenon can hardly be explained other than NH_4NO_3 reduction (eqn (7)) that occurs with influence from the metal oxide. Given the literature's emphasis on the role of acid sites in NH_4NO_3 accumulation on zeolites, a subsequent question is whether the oxide component alters NH_4NO_3 deposit quantities and characteristics within the catalyst and associated with acid sites, and if so, by what means. In the present work, we challenged ourselves with answering the abovementioned questions.

In this work, we used a series of temperature-programmed desorption (TPD) analyses to characterize the nature of NH_4NO_3 deposits and their decomposition in the composite catalysts. We employed two TPD approaches to differentiate NH_4NO_3 decomposition chemistry based on how NH_4NO_3 is deposited in the catalyst, which are described as follows:

(i) Fast-SCR-TPD, where NH_4NO_3 is deposited *in situ* at low-temperature under “fast” SCR reaction conditions, *i.e.*, $[\text{NO}] = [\text{NO}_2] = \frac{1}{2} [\text{NH}_3]$. This allows for characterizing NH_4NO_3 deposits that accumulate on the catalyst under reaction conditions, including “inside” the zeolite component.

(ii) NH_4NO_3 -TPD, where dry NH_4NO_3 solid is physically mixed (*i.e.*, *ex situ* deposition) with the catalyst powder. This allows for characterizing NH_4NO_3 deposits that are not formed under reaction conditions and thus not closely associated with catalyst active sites.

These analyses show that two (2) types of NH_4NO_3 deposits form on Cu-SSZ-13 under low-temperature fast-SCR reaction conditions: Lewis-acid-bound (*i.e.*, Cu-bound) that are highly stable and Brønsted-acid-bound that are moderately stable. On the composite SCR catalyst, a third type of NH_4NO_3 deposit is formed, which we call ‘loosely’ bound NH_4NO_3 owing to its similarity to NH_4NO_3 impregnated directly on the catalyst, that are less stable and decompose at lower temperature than acid bound NH_4NO_3 . Importantly, we show that the composite catalyst facilitates both reduced total NH_4NO_3 deposits and deposits that are either Brønsted-acid-bound or ‘loosely’ bound, thus avoiding highly stable Cu-bound NH_4NO_3 deposits.

Experimental

Synthesis of composite catalysts

Ceria-manganese oxide (CM, Ce-to-Mn molar ratio = 7:3) was prepared *via* thermal decomposition of an aqueous mixture of 4.08 g of $\text{Ce}(\text{NO}_3)_3 \cdot 6\text{H}_2\text{O}$ (Sigma-Aldrich) and 1.18 g of $\text{Mn}(\text{NO}_3)_2 \cdot x\text{H}_2\text{O}$ (Sigma-Aldrich) at 650 °C for 4 h. H-SSZ-13 zeolite (HSZ, Si/Al = 12) was prepared *via* calcination of NH_4^+ -SSZ-13, prepared *via* subsequent steps of hydrothermal synthesis to form the parent zeolite (*i.e.*, Na-SSZ-13) and ion-exchange with NH_4NO_3 . Cu-SSZ-13 (CSZ, Cu ~1.4 wt%) was prepared by subjecting NH_4^+ -SSZ-13 to aqueous ion-exchange

with the Cu precursor. Details on the synthesis procedure are found in our previous work.³²

Composite CM/CSZ or CM/HSZ catalysts (CM, CSZ and HSZ refer to ceria-manganese oxide, Cu-SSZ-13 and H-SSZ-13 components, respectively) were prepared *via* a ball-milling technique. In a typical procedure, 0.4 g of component mixture of CM + HSZ or CM + CSZ, 6 g of isopropanol (Sigma-Aldrich) and 40 g of zirconia beads were milled at 50 rpm for 2 h. Then, the catalyst mixture was dried at 70 °C overnight and subsequently calcined at 450 °C for 4 h. The composite catalysts were prepared at an oxide-to-zeolite weight ratio (O:Z) of 1:3, and we also compare results with O:Z = 1:1 and 3:1. We previously reported the textural properties of the individual components and the composite catalysts and the SEM images of the composite catalysts.³²

Temperature-programmed desorption analysis

Reaction and TPD analyses were carried out in a fixed-bed reactor comprising a vertically mounted quartz tube (9.5 mm ID). Catalyst temperature was monitored with a K-type thermocouple placed upstream of the catalytic bed and controlled with a PID-controlled tubular furnace. The gas composition was measured with a MultiGas™ 2030 FTIR continuous gas analyzer (MKS Instrument), and the feed gas was controlled by a set of Brooks 5850E Series mass flow controllers and a Chromtech HPLC pump for water addition. In a typical experiment, 0.15 g of catalyst (pressed, crushed and sieved at 60–80 mesh) was loaded into the reactor, and the total reactant flow rate was set at 1 L min⁻¹ (mass space velocity = 400 L g⁻¹ h⁻¹).

For “fast” SCR exposure, the catalyst was first pretreated at 550 °C for 1 h in 15% O₂, 8% CO₂ and 6% H₂O (balanced by N₂) and then exposed to a fast SCR feed to generate NH_4NO_3 *in situ*; feed conditions were 175 ppm NO, 175 ppm NO₂, 350 ppm NH₃, 15% O₂, 8% CO₂ and 6% H₂O (balanced by N₂) at 160 °C for 2 h. For TPD analysis following the “fast” SCR exposure, the catalyst was cooled down to 100 °C under a N₂ purge, and then TPD analysis was carried out in N₂ flow by heating the catalyst to 600 °C at a rate of 10 °C min⁻¹. In the TPD results shown below, this is referred to as fast-SCR-TPD analysis. TPD analysis following “standard” SCR exposure was conducted in a similar fashion but replacing equimolar amounts of NO and NO₂ with only 350 ppm NO. In the results below, this is referred to as std-SCR-TPD analysis.

For TPD analysis following solid NH_4NO_3 exposure, 0.05 g of solid NH_4NO_3 (Sigma Aldrich, pre-dried 24 h in N₂ flow at 70 °C) was physically mixed with 0.145 g of catalyst with a mortar and pestle. Once the catalyst- NH_4NO_3 mixture was loaded into the reactor, the TPD analysis was run by heating the mixture to 600 °C at a rate of 10 °C min⁻¹ in N₂ flow. No pretreatment was performed prior to the analysis. In the case of the dual-component (oxide-zeolite) system, the bed composition for the analysis was a mixture of CM powder + zeolite powder (CM/zeolite weight ratio = 1:3) + NH_4NO_3



solid which was physically mixed with a mortar and pestle. This ensures more even NH_4NO_3 interactions with the two catalyst phases. To differentiate this mixture from the ball-milled counterpart (CM/HSZ or CM/CSZ), we denote it as “CM + HSZ” or “CM + CSZ”. In the results shown below, this is referred to as NH_4NO_3 -TPD analysis.

NH_3 -TPD analysis was carried in the absence of SCR reactions (*i.e.*, without NO_x) to compare the NH_3 storage. In a typical analysis, the catalyst was initially pre-exposed to 350 ppm NH_3 , 15% O_2 , 8% CO_2 and 6% H_2O (balanced by N_2) at 160 °C until NH_3 saturation. Then, the catalyst was purged with N_2 and cooled down to 100 °C. Finally, the desorption step was carried out in N_2 flow by heating the catalyst to 600 °C at a rate of 10 °C min^{-1} . Prior to the analysis, the catalyst was pretreated at 550 °C for 1 h in 15% O_2 , 8% CO_2 and 6% H_2O (balanced by N_2).

“Fast” SCR kinetics

In a typical experiment, a diluted catalyst mixture containing 1.5 mg of catalyst, 13.5 mg of $\alpha\text{-Al}_2\text{O}_3$ (Alfa Aesar) and 300 mg of SiO_2 (Sigma-Aldrich) was used. The catalyst bed was initially exposed to a 1 L min^{-1} flow of 15% O_2 , 8% CO_2 and 6% H_2O (balanced by N_2) at 550 °C for 1 h. Then, 175 ppm NO, 175 ppm NO_2 and 350 ppm NH_3 gases were added to the mixture while the reactor cooled down to 320 °C, and testing was performed isothermally for 1 h at various temperatures from 320–120 °C. The kinetic analysis was performed within the range of 280–200 °C, and the reaction turnover rate (TOR) is expressed in mmol NO mol per Cu per s.

Results

Fast SCR exposure

We first focus our attention on the storage phase of the fast SCR TPD measurement, *i.e.*, during “fast” SCR exposure at 160 °C. Fig. 2A–C show NO, NO_2 , N_2O , and NH_3 species evolutions from CM, HSZ, and CSZ during this exposure. CM results in Fig. 2A show immediate and steady outputs of ~20 ppm N_2O and ~150 ppm NH_3 indicating that NH_3 is not stored and NH_4NO_3 does not accumulate on CM. Interestingly, NO and NO_2 evolution from CM suggests nitrite/nitrate accumulation that reaches a saturation threshold, as indicated by an NO_2 inflection at ~2800 s. Next, HSZ results in Fig. 2B show, as expected, significant NH_3 storage, and the pattern of NO and NO_2 evolution and inflection in the NO_2 trace at ~1400 s suggests NH_4NO_3 deposition occurring through ~1400 s. It is worth noting that no N_2O is generated from HSZ at this temperature suggesting that thermal decomposition of NH_4NO_3 does not occur. Lastly, the CSZ results in Fig. 2C show NO and NO_2 evolution similar to HSZ. However, the lack of a clear NO_2 inflection and its continued rise through the duration of the test suggests that NH_4NO_3 deposition occurs for a longer duration on CSZ, indicating that it accumulates for a longer duration on the zeolite with Cu present. Additionally, little

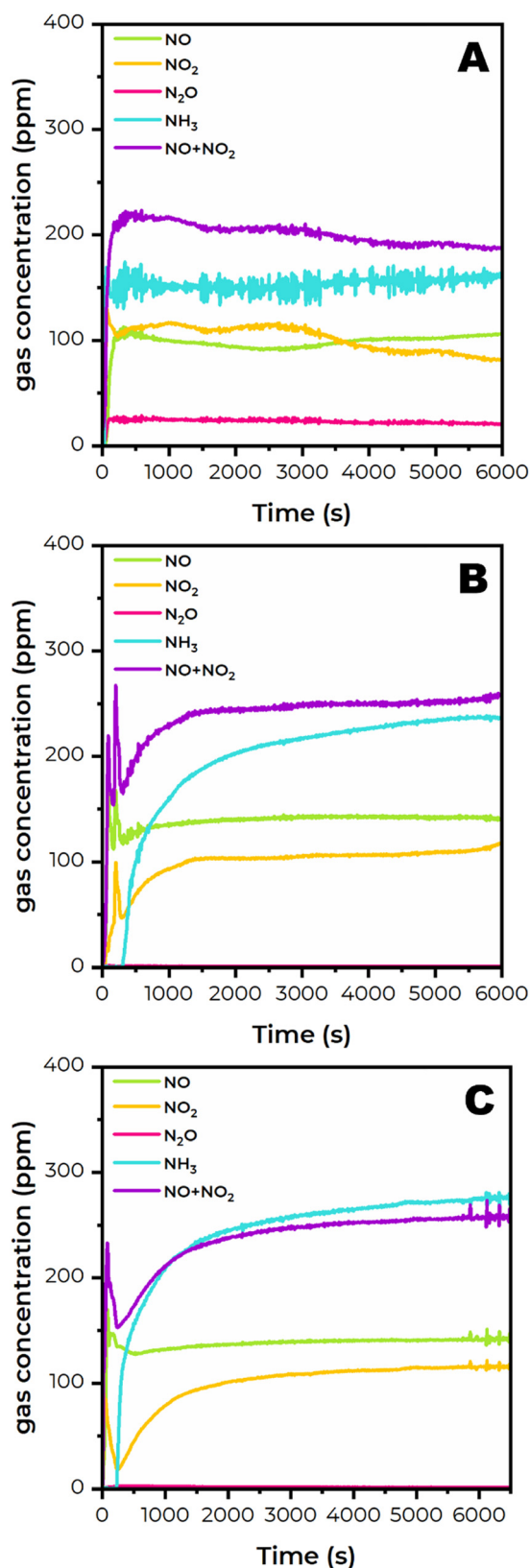


Fig. 2 NO_x and NH_3 evolution from CM (A, top), HSZ (B, middle), and CSZ (C, bottom) during “fast” SCR exposure at 160 °C.



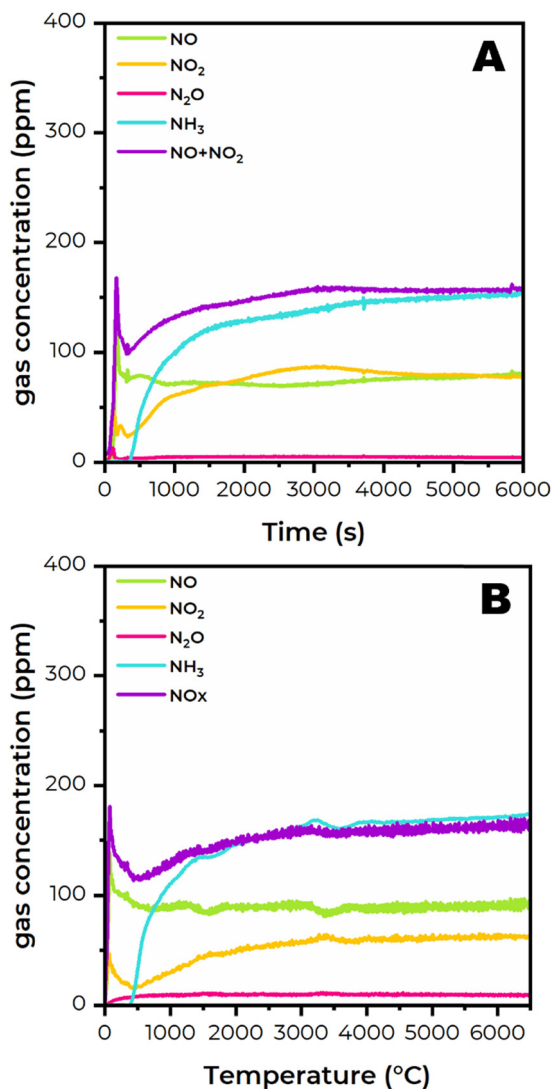


Fig. 3 NO_x and NH₃ evolution from CM/HSZ (A, top) and CM/CSZ (B, bottom) during “fast” SCR exposure at 160 °C.

N₂O evolution suggests negligible NH₄NO₃ decomposition on CSZ at this temperature.

Fig. 3 shows the evolution of NO, NO₂, N₂O, and NH₃ from the composite catalysts CM/HSZ and CM/CSZ (both O:Z = 1:3), respectively, over the course of “fast” SCR exposure at 160 °C. CM/HSZ results in Fig. 3A show NO₂ evolution that is quite instructive. Two inflections in the NO₂ evolution are apparent: a sharp inflection at ~800 s after which NO₂ continues to rise slowly, and a broad inflection at ~3100 s after which NO₂ slightly declines. The broad inflection at ~3100 s we confidently attribute to nitrite/nitrate species saturation on the CM component like in Fig. 2A; the sharp NO₂ inflection at ~800 s we believe is, like HSZ, NH₄NO₃ deposition occurring rapidly to saturation at ~800 s. The latter is corroborated by N₂O evolution slowly increasing to ~5 ppm at ~800 s and then steadying. These results indicate that NH₄NO₃ deposition occurs for a shorter duration on HSZ with CM present. CM/CSZ results in Fig. 3B show two

inflections in the NO₂ evolution profile: one at ~1600 s after which NO₂ continues to rise slowly, and one at ~3300 s after which NO₂ steadies. The latter, similar to CM/HSZ, we confidently attribute to nitrite/nitrate species saturation on CM, and the former we attribute to NH₄NO₃ accumulation through ~1600 s. N₂O evolution is higher at 10 ppm from CM/CSZ, indicating even greater decomposition of NH₄NO₃ occurs on CSZ (*versus* HSZ) with CM present at this temperature.

Importantly, the results in Fig. 3 confirm that NH₄NO₃ deposition at this temperature occurs for a shorter duration, and likely at reduced quantity, on CM/CSZ *versus* CSZ, which will be confirmed later. These results also indicate that nitrite/nitrate species take longer to saturate on CM in the composite catalysts suggesting that some of these species are titrated from the CM surface in the composite catalysts. We believe that the slower deposition of NH₄NO₃ on Cu sites *versus* Brønsted-acid sites in CSZ and CM/CSZ is related to differences in the reactivity of surface nitrates. This was demonstrated by Votsmeier,³³ who showed that NO₂ disproportionation/oxidation products are displaced more rapidly by NH₃ on Cu sites than nitrate species on Al sites, and corroborated by Liu *et al.*³⁴ who demonstrated differences in NH₃ evolution from Cu *versus* Brønsted-acid sites following NO + O₂ exposure, both of which will be discussed further later.

Fast-SCR-TPD analysis

We next turn our attention to the TPD portions of the analyses. Fig. 4 shows the results of fast-SCR-TPD analysis of CM, HSZ, and CM/HSZ (O:Z = 1:3), including NO, NO₂, N₂O, and NH₃ evolution. This enabled us to characterize NH₄NO₃ deposits that accumulated throughout the catalyst and in close proximity to active sites inside the zeolite during “fast” SCR exposure. The CM component in Fig. 4A demonstrates primarily NO₂ release from the oxide surface *via* desorption of surface “nitrates” formed on CM. Wu *et al.* observed similar NO₂ evolution over ceria–manganese oxide during NO₂-TPD analysis that they ascribed to monodentate/bidentate nitrates and ionic nitrates (NO₃[−]), respectively.³⁵ Minor evolution of N₂O and the lack of NH₃ evolution suggest little accumulation of NH₄NO₃ on the oxide surface which is consistent with Fig. 2A. NO evolution at high-temperature is likely due to the thermodynamically-driven NO₂ reduction (2NO₂ ⇌ 2NO + O₂) above ~350 °C.³⁶ The minor evolution and then waning of N₂O occurs in the same temperature range where we previously observed CM to shift from catalyzing reducing reactions to oxidizing reactions and aligns with our prior ascription of N₂O evolution from CM < 200 °C to thermal decomposition of NH₄NO₃.³² We believe that this holds true here as well.

Fast-SCR-TPD analysis results from HSZ in Fig. 4B show large N₂O evolution at 276 °C, suggesting predominantly NH₄NO₃ decomposition *via* eqn (4). NH₄NO₃ decomposition can occur purely thermally, or catalytically by acid sites. From



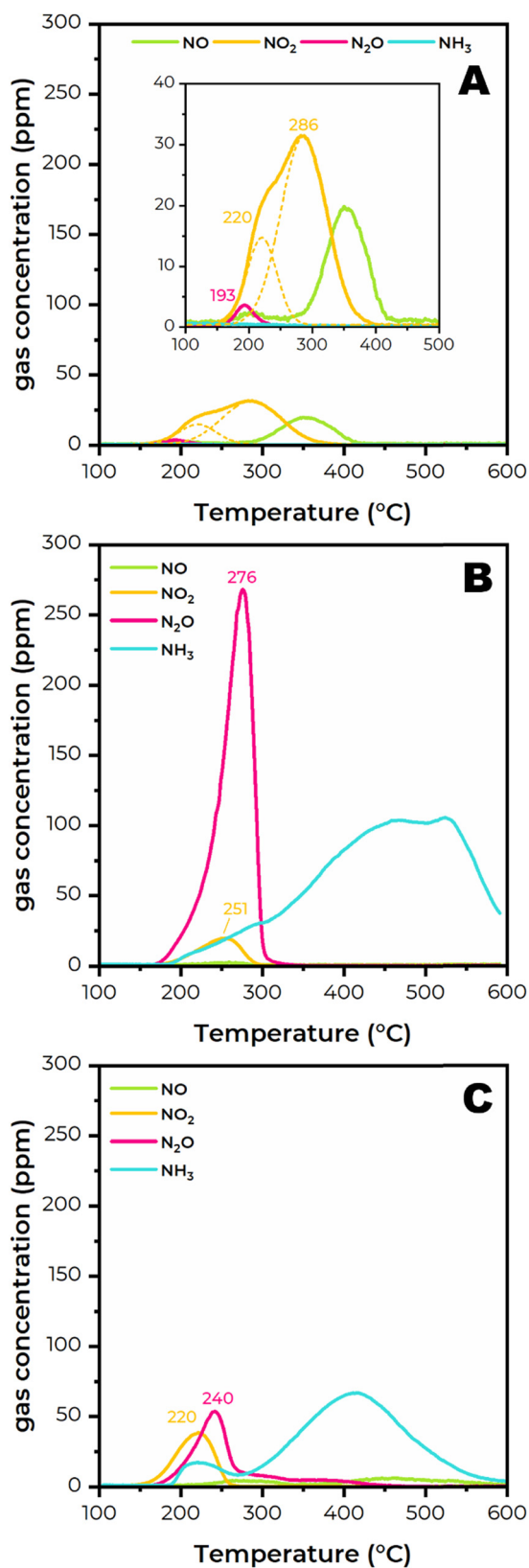
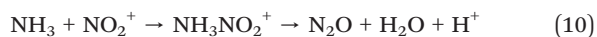
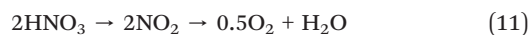


Fig. 4 Fast-SCR-TPD analysis of CM (A, top), HSZ (B, middle), and CM/HSZ (C, bottom).

the literature, where this reaction is catalyzed by Brønsted-acid sites (BAS), it occurs *via* the following steps:^{37–39}



NO_2 evolution is also observed at similar temperature but much lower intensity *versus* N_2O , and thus likely similarly originating from NH_4NO_3 decomposition. We believe that NO_2 evolves from NH_4NO_3 dissociation to NH_3 and HNO_3 (eqn (3)), followed by HNO_3 dissociation to NO_2 :^{16,40}



To confirm the little influence of adsorbed NH_3 on the N_2O and NO_2 evolution from HSZ during fast-SCR-TPD, NH_3 evolution from Fig. 4B is compared with NH_3 evolution from NH_3 -TPD analysis on HSZ and the results are shown in Fig. S1.† The NH_3 desorption profiles from both studies are strikingly similar and show NH_3 evolution with maximum intensity at ~ 450 °C indicative of BAS-bound NH_3 species. The modest difference in magnitude at high temperature is attributed to reduced NH_3 storage under fast-SCR reaction conditions. This provides evidence that the N_2O and NO_2 products in Fig. 4B originate from NH_4NO_3 decomposition.

Fig. 4C shows the fast-SCR-TPD analysis of the H-form composite catalyst (CM/HSZ). N_2O evolution from CM/HSZ is similar to the H-form zeolite (HSZ) but at reduced intensity and apparent reduced temperature. The reduced intensity indicates reduced accumulation (*i.e.*, quantity) of NH_4NO_3 in the presence of CM which is consistent with the observations from Fig. 3A. The reduced temperature appears to result from CM influence on the nature of NH_4NO_3 deposits as well. It is unclear if the deposits from HSZ and CM/HSZ are distinct from one another; this will be revisited later. NO_2 evolution also occurs on the composite CM/HSZ catalyst but at lower temperature *versus* HSZ; this is likely contributed by CM (*vide* Fig. 4A) but the increased intensity suggests that NO_2 , at least in part, derives *via* influence from the CM component on NH_4NO_3 deposits. It is worth noting that the lack of higher temperature NO_2 evolution from CM/HSZ (*e.g.*, that was observed from CM in Fig. 4A) suggests that surface ‘nitrate’ species were titrated from the CM surface during fast-SCR before becoming more recalcitrant, analogous to what we demonstrated in prior work.³² High temperature NH_3 evolution from CM/HSZ centered at ~ 410 °C indicates BAS-bound NH_3 species, but the small NH_3 peak at ~ 220 °C which coincides with NO_2 evolution further corroborates CM-influenced NH_4NO_3 dissociation (eqn (3)) on HSZ. To confirm this, NH_3 evolution from CM/HSZ was compared during fast-SCR-TPD analysis (Fig. 4C) with NH_3 -TPD analysis and the results are shown in Fig. S2.† The NH_3 desorption profiles from both studies are similar apart from the NH_3 peak at

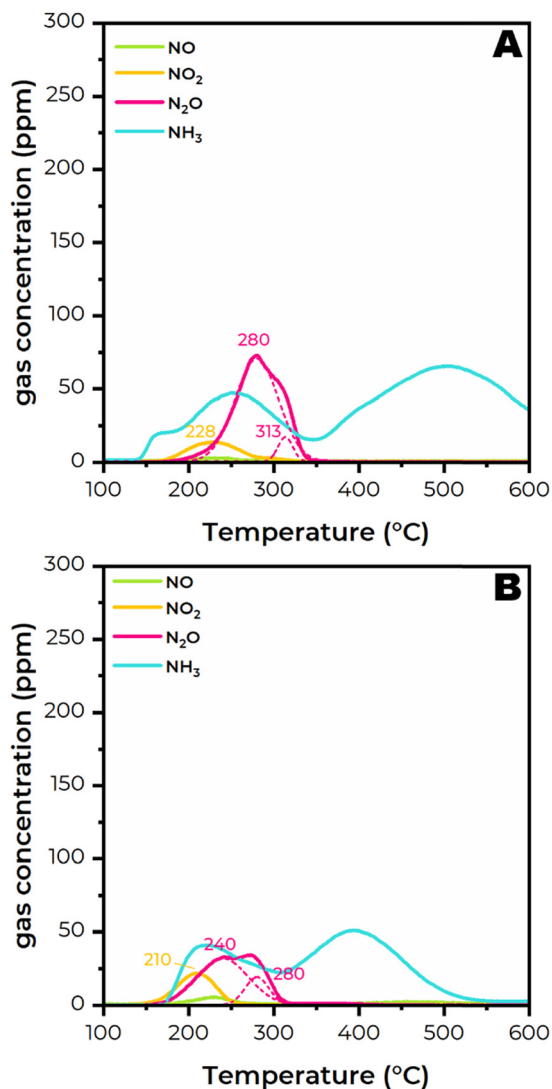


Fig. 5 Fast-SCR-TPD analysis of CSZ (A, top) and CM/CSZ (B, bottom).

~220 °C mentioned above. This confirms the hypothesis stated above that the NH_3 peak at ~220 °C originates from NH_4NO_3 dissociation which further corroborates the source of NO_2 evolution in Fig. 4C.

Fig. 5 shows NO_x and NH_3 evolution during fast-SCR-TPD analysis of the Cu-form catalysts, CSZ and CM/CSZ (O:Z = 1:3). N_2O evolution from CSZ (Fig. 5A) is much smaller than HSZ and indicates that Lewis acid sites (LAS, *i.e.*, Cu) reduce NH_4NO_3 accumulation in-line with the results from Grönbeck *et al.*^{37–39} However, importantly, the bimodal nature of the N_2O evolution from the Cu-form catalysts sheds additional light on both origins of NH_4NO_3 formation. This will enable us to clearly ascertain the impact of CM, which will be discussed later. However, the bimodal nature of N_2O evolution in these catalysts is discussed here. Olsson *et al.* showed that, upon TPD analysis after exposure to $\text{NO}_2 + \text{NH}_3 + \text{O}_2 + \text{H}_2\text{O}$ at 150 °C, Cu-SSZ-13 yielded a single N_2O evolution feature centered at 282 °C (similar to HSZ in Fig. 4B).⁴¹ They also found that NH_4NO_3 binds more strongly

to Cu *versus* BAS. In comparison, Xi *et al.* showed that Cu-SSZ-13, upon TPD analysis after exposure to $\text{NO}_2 + \text{NH}_3 + \text{O}_2 + \text{CO}_2 + \text{H}_2\text{O}$ at 200 °C, yielded a single N_2O evolution feature centered at ~314 °C.⁴² We believe that the nature of NH_4NO_3 deposits formed in these two references is distinct from one another, and that they are differentiated by the temperature at which they are formed which governs their location and degree of stabilization. We believe that the NH_4NO_3 formed at 150 °C in the Olsson *et al.* work is primarily bound to BAS (weaker) whereas the NH_4NO_3 formed at 200 °C in the Xi *et al.* work is primarily bound to Cu (stronger). This can be rationalized by relative contributions of LAS-bound and BAS-bound NH_3 on SCR at 150 °C *versus* 200 °C. In our work, there is evidence of both BAS-bound and Cu-bound NH_4NO_3 deposits as seen by the bimodal nature of N_2O evolution in Fig. 5A. The significance of this will become apparent when we show the results from the CM/CSZ composite catalyst.

Fig. 5A also shows that NH_3 evolution during fast-SCR-TPD from CSZ occurs as early as 150 °C which we ascribe to early dissociation of NH_4NO_3 to NH_3 and HNO_3 . To help clarify this, in Fig. S3† we compare NH_3 evolution from CSZ during fast-SCR-TPD analysis, std-SCR-TPD analysis, and NH_3 -TPD analyses. The NH_3 desorption profiles from all three studies are similar and demonstrate a bimodal profile that includes high temperature desorption of BAS-bound NH_3 species and lower temperature (250–280 °C) desorption of LAS-bound NH_3 species. These results confirm our prior assignment of the initial NH_3 evolution to early dissociation of NH_4NO_3 and the remainder to LAS- and BAS-bound NH_3 species.

Fig. 5B shows that N_2O evolution during fast-SCR-TPD analysis from CM/CSZ is smaller and occurs at lower temperature *versus* CSZ. This is analogous to CM/HSZ *versus* HSZ but differs in that N_2O release from CSZ is much less prominent than HSZ because of reduced NH_4NO_3 accumulation with Cu present. What is immediately evident is the lack of N_2O evolution at ~313 °C which, importantly, indicates no Cu-bound NH_4NO_3 deposits in the CM/CSZ catalyst. What is similarly noteworthy is the shift of a significant portion of the N_2O evolution from 280 °C to 240 °C with CM addition. This is consistent with the impact of CM on HSZ that was observed in Fig. 4, and this confirms that the NH_4NO_3 deposits that yield N_2O evolution at 240 °C and 280 °C are in-fact distinct in nature. Additionally clarity comes from the results of Liu *et al.*; Liu *et al.* looked at NH_4NO_3 decomposition of NH_4NO_3 -impregnated H-SSZ-13 under He purging and showed that this NH_4NO_3 decomposed at ~240 °C (yielding N_2O and NO_x species).³¹ Since NH_4NO_3 impregnation results in ‘loosely’ bound, or destabilized, NH_4NO_3 deposits, the results of Liu *et al.* confirm that the N_2O evolution features at ~240 °C in the fast-SCR-TPD profiles above are associated with destabilized NH_4NO_3 . Collectively, we believe that this provides evidence of three (3) types of NH_4NO_3 deposits found on the catalysts which are summarized in Table 1.



Table 1 Types of NH_4NO_3 deposits found on HSZ, CSZ, CM/HSZ and CM/CSZ

Nature of NH_4NO_3	Peak decomposition temperature	Catalysts observed on	Ref.
Cu-bound	314 °C	CSZ	Xi <i>et al.</i> ⁴²
BAS-bound	280 °C	HSZ, CSZ, CM/CSZ	Han <i>et al.</i> ⁴¹
Destabilized, or 'loosely' bound	240 °C	CM/HSZ, CM/CSZ	Liu <i>et al.</i> ³¹

These findings, and particularly the diverse N_2O release profiles, provide clear indication that CM influences the location (and stability) of NH_4NO_3 deposits that form in the catalyst. In the absence of CM on CSZ, highly stable Cu-bound NH_4NO_3 (similar to what Xi *et al.*⁴² observed after $\text{NO}_2 + \text{NH}_3$ exposure at 200 °C) are apparent which decompose at ~314 °C. With CM present (*i.e.*, on CM/CSZ), it is clear that these deposits are not present. The results from Fig. 2C showed that NH_4NO_3 deposits take longer to stabilize with Cu present, and thus we believe that Cu-bound NH_4NO_3 is slower to form and susceptible to greater influence from CM. Next, also on CSZ without CM, aside from Cu-bound NH_4NO_3 the only other NH_4NO_3 evident is BAS-bound (similar to what Han *et al.*⁴¹ observed after $\text{NO}_2 + \text{NH}_3$ exposure at 150 °C) which decomposes at ~280 °C. With CM present, it is similarly clear that a portion of these deposits are destabilized, *i.e.*, they are shifted to a form (*i.e.*, chemistry and/or location) where they are no longer stabilized as BAS- or LAS-bound deposits. The NO_2 evolution in Fig. 5B from CM/CSZ is similar to what was observed from CM/HSZ in Fig. 4C, and we believe provides indication of the pathway of CM influence on NH_4NO_3 decomposition. The NH_4NO_3 -TPD analyses that follow are intended to provide further clarity to the latter.

Finally, NH_3 evolution from CM/CSZ during fast-SCR-TPD analysis (Fig. 5B) was compared with std-SCR-TPD and NH_3 -TPD analyses, and the results are shown in Fig. S4.† The NH_3 desorption profiles from the std-SCR-TPD and NH_3 -TPD analyses demonstrate solely bimodal LAS- and BAS-bound NH_3 species, analogous to CSZ. This confirms our assignment of the initial NH_3 evolution (~150 °C) from CSZ to early dissociation of NH_4NO_3 . However, low temperature NH_3 release from fast-SCR-TPD is shifted to lower temperature and very similar to low-temperature NH_3 release from CM/HSZ. Above, we ascribed the latter to NH_4NO_3 dissociation; we believe that this holds true here as well but with likely some inevitable influence from Cu.

To gain further insight into the influence of CM on NH_4NO_3 deposits formed on CSZ during the fast SCR reaction, fast-SCR-TPD analysis was performed on CM/CSZ with O:Z = 1:1 and 3:1, and the results are shown in Fig. S5† together with O:Z = 1:3 (from Fig. 5B) at a common scale. The results for O:Z = 1:1 in Fig. S5B† show that the behavior for all species is very similar to O:Z = 1:3 in Fig. S5A.† The N_2O release from decomposition of 'loosely' bound and BAS-bound NH_4NO_3 deposits has shifted slightly to lower temperature, and their quantity appears shifted to a majority of 'loosely' bound; this suggests even stronger influence of CM on NH_4NO_3 deposits formed. A third N_2O feature is

observed at 376 °C that we attribute to CM-catalyzed NH_3 oxidation due to its profile matching exactly the NH_3 release at this temperature. Although there is no O_2 in the gas stream during the TPD, the large fraction of CM likely retains sufficient oxidation capacity. Interestingly, at an increased scale we see that this N_2O feature is present at O:Z = 1:3 but at a significantly reduced magnitude, suggesting a superior coupling of oxide to zeolite at O:Z = 1:3 for minimizing non-selective NH_3 oxidation. The results for O:Z = 3:1 in Fig. S5C† show that N_2O release from decomposition of NH_4NO_3 deposits shifted to even lower temperature. The results from this sample appear to be dominated by the CM phase, which is expected. The main N_2O feature from NH_4NO_3 decomposition at 202 °C coincides with the primary release of surface nitrite species from CM as observed in Fig. 4A. Also, interestingly, the higher temperature release of stable nitrates from CM observed in Fig. 4A at 286 °C is not evident in Fig. S5C,† emphasizing our results reported prior to the titration of surface nitrites from the CM surface with zeolite present before they transform into stable nitrate species.³²

NH_4NO_3 -TPD analysis

In this section, we provide the results from NH_4NO_3 -TPD analysis to confirm and corroborate the results presented previously regarding the nature and observance of 'destabilized' NH_4NO_3 deposits. Fig. 6 shows NO_x and NH_3 evolution during NH_4NO_3 -TPD analysis over SiO_2 and CM. The TPD analysis with SiO_2 shown in Fig. 6A serves as a baseline experiment representing a noncatalytic thermal NH_4NO_3 decomposition. Thermal decomposition of solid NH_4NO_3 over SiO_2 largely results in NH_3 and is indicative of NH_4NO_3 dissociation according to eqn (3). This finding confirms that the evolution of NO_x (*e.g.*, N_2O and NO_2) is catalytically derived in the course of NH_4NO_3 decomposition previously observed. The low temperature of NH_4NO_3 decomposition at 206 °C also confirms the results from Pereira *et al.* who hypothesized the confinement effect that zeolite has on NH_4NO_3 , in that NH_4NO_3 is not easily vaporized when "trapped" in the zeolite cage and thus disfavoring dissociation to gaseous NH_3 and HNO_3 .¹⁶ Aside from NH_4NO_3 dissociation, noncatalytic NH_4NO_3 decomposition is also accompanied by NH_4NO_3 sublimation (eqn (2)) that was supported by post-analysis of white solid deposits that were formed at the unheated part of the downstream reactor outlet.

NH_4NO_3 -TPD analysis on CM (Fig. 6B) exhibits both NH_3 and NO_x evolution. The temperature of peak NH_4NO_3 decomposition over CM is consistent with SiO_2 and further



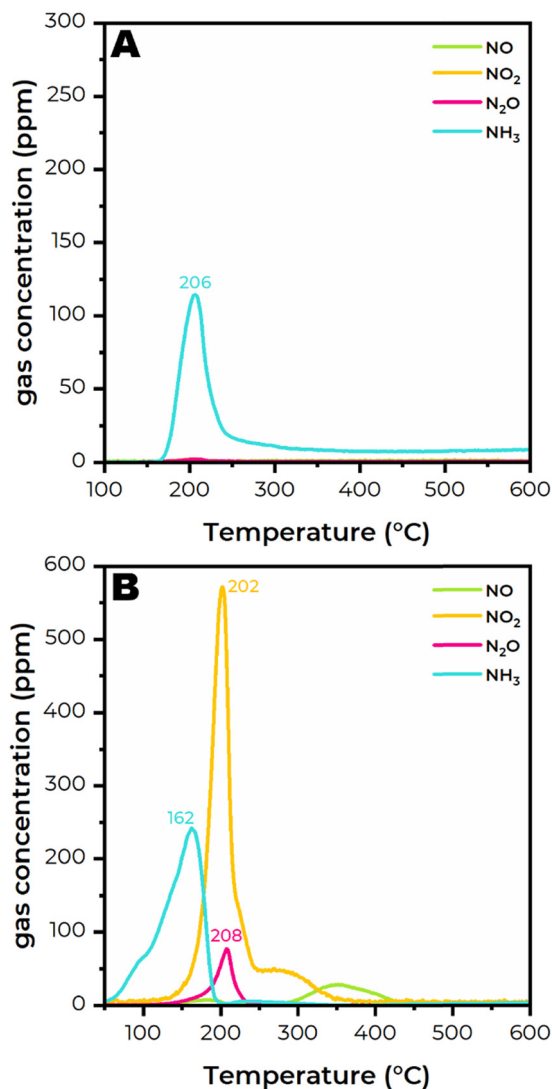


Fig. 6 NH₄NO₃-TPD analysis on SiO₂ (A, top) and CM (B, bottom).

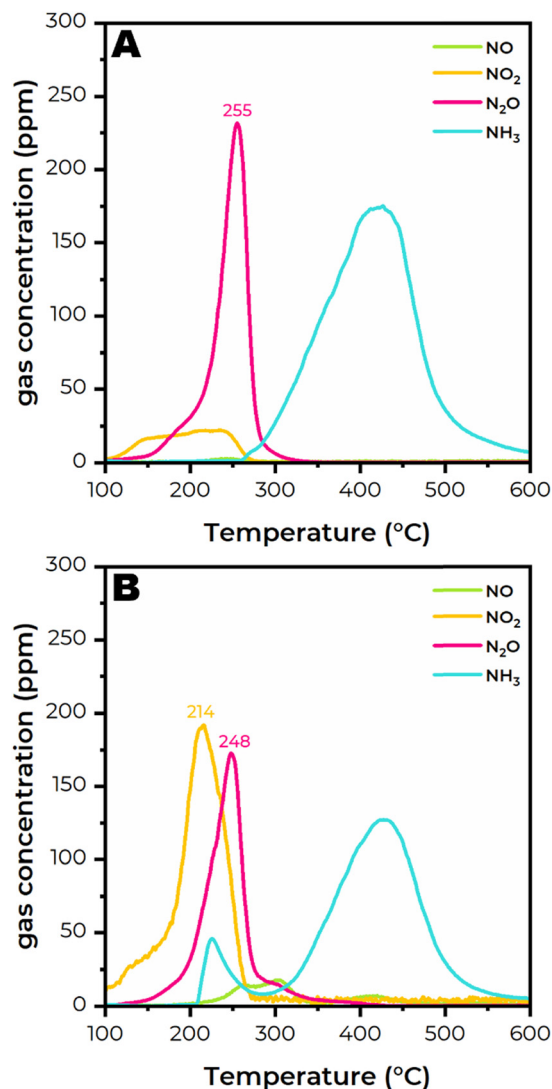


Fig. 7 NH₄NO₃-TPD analysis on HSZ (A, top) and CM + HSZ (B, bottom).

confirms the role of confinement effects on NH₄NO₃ decomposition in the presence of zeolite. In contrast, NH₃ evolution over CM is unique *versus* the baseline experiment with SiO₂ in that it emerges as early as at 50 °C and proceeds to a peak at 162 °C *versus* 206 °C on SiO₂. This indicates that CM catalyzes early NH₄NO₃ dissociation to NH₃ and HNO₃ (eqn (3)) with HNO₃ stored on CM at low temperature.

As the temperature increases, the remarkable evolution of NO₂ from CM shown in Fig. 6B further reconfirms the role of CM in catalyzing HNO₃ decomposition to NO₂ (eqn (11)). We believe that this is instructive towards understanding the ability of CM to catalyze NH₄NO₃ dissociation to NH₃ and HNO₃. N₂O and NO are also observed from CM, but their intensity is small compared to NH₃ and NO₂. Compared to the fast-SCR-TPD analysis of CM (Fig. 4A), the NH₄NO₃-TPD analysis of CM is consistent in that NO₂ is the dominant desorption product, and N₂O and NO are the minor effluents. The major difference between the two analyses is the NH₃ evolution. The fact that NH₃ is released below 160 °C

confirms that CM lacks adsorption/storage sites to retain the NH₃ dissociation product and, compared to Fig. 4A, confirms little accumulation of NH₄NO₃ on CM directly during “fast” SCR.

Fig. 7A shows the results of NH₄NO₃-TPD analysis of HSZ. NO_x/NH₃ evolution from HSZ is remarkably similar to its fast-SCR-TPD analysis (Fig. 4B) in both magnitude and in that N₂O remains the main NO_x desorption product. However, despite their similarities, N₂O desorption occurs at noticeably lower temperature for NH₄NO₃-TPD *versus* fast-SCR-TPD analysis. NO₂ also evolves from HSZ at a noticeably lower onset temperature in NH₄NO₃-TPD than in fast-SCR-TPD. Collectively, these results suggest differences in the stability of NH₄NO₃ toward dissociation and support the argument that, in the case of *in situ* deposition during fast-SCR, the NH₄NO₃ is ‘stabilized’ at BAS inside of the zeolite and more recalcitrant toward decomposition. It is also feasible that NH₄NO₃ deposits formed during fast-SCR and



strongly bound to BAS retard NH_4NO_3 decomposition by inhibiting the activity of the acid site. This could occur physically by occlusion or could occur through inhibiting dissociation of NH_4NO_3 or inhibiting subsequent protonation of HNO_3 to form NO_2^+ *via* eqn (9) (which precedes N_2O formation). Regardless, the subsequent impact is the same: NH_4NO_3 deposits formed under fast-SCR conditions are stabilized and more resistant to decomposition. In the case of external NH_4NO_3 deposits (*i.e.*, NH_4NO_3 -TPD), NH_3 and HNO_3 are likely readily formed *via* dissociation and subsequently uninhibited leading to a lower decomposition temperature, potentially through interactions with comparatively uninhibited BAS. The difference in decomposition temperature of impregnated NH_4NO_3 on HSZ in Fig. 7A (that decompose at 255 °C) and ‘destabilized’ NH_4NO_3 (*e.g.*, Fig. 4C for CM/HSZ that decompose at 240 °C) is likely an effect of proximity of NH_4NO_3 in relation to the uninhibited BAS with potential minor influence from CM. Lastly, the release of NH_3 at high temperatures (>250 °C) indicates that NH_4NO_3 dissociation-derived NH_3 is stored over BAS, likely during the low-temperature desorption phase, and then re-released during the high-temperature desorption phase.

Fig. 7B shows the results of NH_4NO_3 -TPD analysis on CM + HSZ (O : Z = 1 : 3); here, we compare these results to NH_4NO_3 -TPD analyses on CM and HSZ and to fast-SCR-TPD analysis on CM/HSZ. N_2O evolution during NH_4NO_3 -TPD analyses from CM + HSZ and HSZ is similar and, again, indicative of uninhibited NH_4NO_3 dissociation. In contrast, NO_2 evolution from CM + HSZ is much larger than HSZ and thus the result of CM influence. This is corroborated both by the NO_2 desorption feature from pure CM in Fig. 6B and by the respective magnitude of NO_2 and N_2O desorption features from CM/HSZ in Fig. 4C. The early rise of NO_2 suggests that NH_4NO_3 dissociation to NH_3/HNO_3 and eventually to NO_2 is catalyzed by CM. As the HNO_3 dissociation to NO_2 (eqn (11)) wains, the N_2O signal rises indicating likely the onset reaction of HNO_3 protonation competing with CM-catalyzed dissociation of HNO_3 to NO_2 . The position of the N_2O peak in CM + HSZ is slightly lower than in HSZ only, which we attribute to CM enhancing NH_4NO_3 dissociation to NH_3 and HNO_3 as a precursor to N_2O formation. Impressively, aside from the signal intensity, the desorption features and peak positions in the NH_4NO_3 -TPD profile of CM + HSZ (Fig. 7B) are very similar to the fast-SCR-TPD analysis on CM/HSZ (Fig. 4C), including sequential NO_2 - N_2O evolution at comparable intensities and low-/high-temperature NH_3 features.

The similarity between the data sets in Fig. 7B and 4C suggests that the two samples share the same nature of NH_4NO_3 deposits. In the previous section with fast-SCR-TPD analysis, we showed that NH_4NO_3 formed on HSZ *in situ* under fast-SCR conditions and decomposed without CM present were more stable due to their BAS-bound nature. The current result of NH_4NO_3 -TPD with CM + HSZ reinforces our argument that the low-temperature shift of $\text{N}_2\text{O}/\text{NO}_2$ features

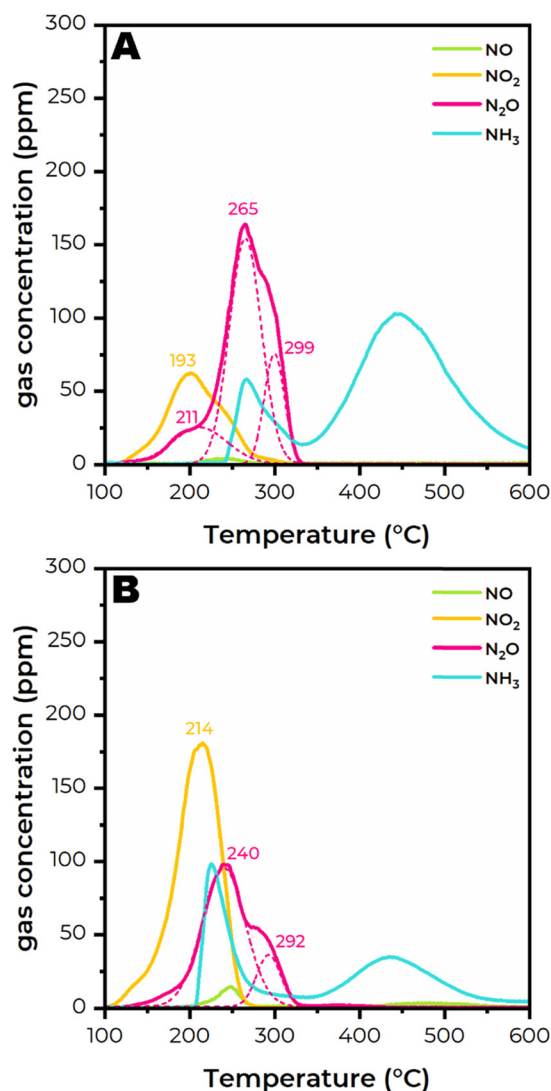


Fig. 8 NH_4NO_3 -TPD analysis on CSZ (A, top) and CM + CSZ (B, bottom).

observed in fast-SCR-TPD of CM/HSZ *versus* HSZ derives from the decomposition of ‘destabilized’ NH_4NO_3 deposits. Lastly, the intensity discrepancy of the CM + HSZ NH_4NO_3 -TPD and CM/HSZ fast-SCR-TPD profiles corroborates reduced NH_4NO_3 formed in the presence of CM during fast SCR in a similar fashion to HSZ *versus* CM/HSZ under fast SCR.

Fig. 8A shows the NH_4NO_3 -TPD analysis results on CSZ. Like HSZ, the NO_x/NH_3 evolution profile is similar to fast-SCR-TPD analysis (Fig. 5A), with N_2O the dominant product. N_2O evolution remains multimodal, yet, in this case, the low-temperature feature (~211 °C) is much more prominent *versus* HSZ. This is also observed in the HSZ NH_4NO_3 -TPD (Fig. 7A). The same phenomenon in HSZ is likely responsible for this feature in CSZ: early activation of HNO_3 (*via* NH_4NO_3 dissociation) by unobstructed BAS. What differentiates the desorption profile of CSZ from HSZ is the low-temperature NO_2 feature (~193 °C), which is much more prominent for CSZ, and the low-temperature NH_3 feature (~266 °C), which



is unique to CSZ. The former feature is likely induced by Cu active sites, and the release mechanism likely occurs *via* uninhibited Cu catalyzed HNO_3 decomposition to NO_2 . The latter feature is likely the release of NH_3 adsorbed from LAS (*i.e.*, Cu) with NH_3 also originating from early dissociation of NH_4NO_3 . The absence of this analogous feature from the fast-SCR-TPD profile of HSZ (Fig. 4B) suggests the involvement of Cu in stabilizing and then releasing NH_3 from NH_4NO_3 dissociation rather than NH_3 produced directly from NH_4NO_3 decomposition/dissociation.

Fig. 8B shows the results of NH_4NO_3 -TPD analysis on CM + CSZ (O:Z = 1:3). Unlike CSZ, NO_2 evolution is the most dominant decomposition product. This low-temperature NO_2 feature shares a similar intensity and peak position to those from NH_4NO_3 -TPD analysis on CM-HSZ (Fig. 7B), thus reconfirming the effect of CM in facilitating both NH_4NO_3 dissociation and HNO_3 decomposition to NO_2 . The latter provides valuable insight into the origins of CM influence on 'destabilized' NH_4NO_3 deposits in the composite catalysts. N_2O evolution is smaller from CM + CSZ *versus* CSZ alone. This is likely because most of HNO_3 derived from noncatalytic NH_4NO_3 dissociation is converted by CM to NO_2 , thus lowering the abundance of the precursor to NO_2^+ necessary for N_2O formation. CM + CSZ exhibits greater low-temperature NH_3 evolution; this appears to derive predominantly from catalytic NH_4NO_3 dissociation aided by CM and release of Lewis/Cu-bound NH_3 species. In comparison with the fast-SCR-TPD analysis of CM/CSZ (Fig. 5B), despite the remarkable difference in intensity, the desorption features as well as peak positions in the NH_4NO_3 -TPD spectra of CM + CSZ are quite comparable including early release of NO_2 and, in particular, the bimodal nature of N_2O release. Such a similarity appears to be consistent for both composite catalytic systems; this suggests that, regardless of the presence of Cu active sites, 'destabilized' NH_4NO_3 deposits are more prominent in the presence of the CM component.

Discussion

It has consistently been reported in the literature that NH_4NO_3 formation over H- and Cu-exchanged zeolites occurs within the zeolite cage over BAS and Cu sites, and the results presented above on HSZ and CSZ confirm this.^{24,25,30,31} In the absence of Cu, our results show that NH_4NO_3 formation occurs quickly on HSZ under "fast" SCR conditions at 160 °C and demonstrate that BAS-bound NH_4NO_3 deposits form which are more stable than unbound deposits. On CSZ and under the same conditions, our results show that NH_4NO_3 formation is reduced in the presence of Cu, confirming what has been observed by others, yet results in Cu-bound deposits being even more stable than BAS-bound deposits and slower to develop.

On the composite catalysts, our results demonstrate that CM prevents Cu-bound deposits from forming which results in even further reduction in total NH_4NO_3 deposits

formed. Furthermore, the persistently similar TPD pattern in fast-SCR-TPD to that in NH_4NO_3 -TPD analysis for composite catalysts indicates that CM facilitates the accumulation of NH_4NO_3 deposits that are comparatively 'destabilized'. A major question then arises as to how CM suppresses NH_4NO_3 accumulation and facilitates their 'destabilized' nature. Here, we believe the NO_2 evolution features with CM present in both the TPD results and under fast SCR reaction conditions (Fig. 1A for the ball-milled sample) above are instructive at understanding both pathways of CM influence on NH_4NO_3 formation and decomposition.

In the previous work with standard SCR reaction, we ascribed the capacity of CM to provide nitrite-like active intermediates such as HONO and N_2O_3 for the reaction to the synergistic effect occurring in the reaction over combined CM-zeolite catalysts.³² Under fast SCR conditions, HONO and N_2O_3 should in theory be more abundant as they are formed due to the reaction of NO and NO_2 in equilibrium with H_2O (eqn (12) and (13)):⁴³



In practice, however, NO_2 consumption for NH_4NO_3 formation/accumulation (eqn (1)) at low temperature proceeds at a much higher rate than NO consumption for the subsequent NH_4NO_3 reduction (eqn (7)). Such a discrepant consumption rate likely prevents NO and NO_2 from coupling with each other and generating desired active intermediates (*i.e.*, N_2O_3) in the absence of CM. Thus, maintaining a balanced rate of consumption of NO and NO_2 is therefore likely key to reducing total NH_4NO_3 buildup in the zeolite and the role that CM assumes. The exact mechanism of how this occurs is unclear, as is the unique influence of CM on NH_4NO_3 accumulation as a function of temperature. However, our previous studies on the low-temperature enhancement observed with the composite catalysts are highly instructive towards this understanding, and we discuss this in further detail here in the context of the present study.³²

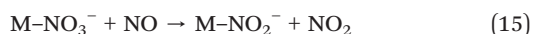
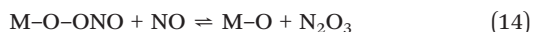
First, in the absence of CM, we previously observed that, at low temperatures, Cu centers in CSZ exhibit NH_3 -induced inhibition which is in-line with what has been reported by others.^{2,3} Thus, at low temperatures (<180 °C), the fast SCR reaction is highly dependent on BAS to drive the reaction, and over-consumption of NO_2 is limiting and thus results in NH_4NO_3 deposits as described above. This explains the preferential formation of NH_4NO_3 deposits at BAS as observed by us in Fig. 4B and Olsson *et al.*⁴¹ At higher temperatures, NH_3 inhibition wains on Cu centers, their involvement in SCR reaction becomes much more significant, and BAS take a passive role in overall SCR. Therefore, as expected, NH_4NO_3 deposits also shift with the SCR reaction to Cu centers where they are more stable. This, similarly,



agrees with our results in Fig. 5A and the results from Xi *et al.*⁴²

With CM present, we believe that reduced NH_4NO_3 buildup occurs through a balanced rate of NO & NO_2 consumption along the same lines as we reported previously, and we expect that this occurs mechanistically similar to what we reported previously: the facile reaction of CM-derived nitrites with the SCR catalyst.³² We previously demonstrated that CM influence on the SCR catalyst at low temperature was confined to SCR involving CM and BAS. This supports the results above that demonstrate CM influence on reducing BAS-bound NH_4NO_3 resulting in increased NH_4NO_3 deposits that are comparatively ‘destabilized’ (Fig. 4C). We also previously demonstrated that at $>180^\circ\text{C}$, CM had greater influence on SCR at Cu centers at these higher temperatures owing to their increased involvement in the SCR reaction.³² Again, this supports the results above that demonstrate CM influence on reducing Cu-bound NH_4NO_3 as shown in Fig. 5. Maintaining a balanced rate of consumption of NO and NO_2 globally within the catalyst is likely key to reducing NH_4NO_3 buildup in the zeolite and the role that CM assumes during the SCR reaction.

NO_2 adsorption/activation on the surface of CM seems to be the key step in both the promotional impact of CM on SCR efficiency and reducing NH_4NO_3 deposits. Over ceria-based catalysts NO_2 is predominantly adsorbed as nitrates. Depending on how they are bonded to the surface, nitrates can exhibit various thermal stabilities, ranging from ligated nitrates (*e.g.*, monodentate/ bidentate nitrates) with lower desorption temperature (peak at $\sim 220^\circ\text{C}$, Fig. 4A) to ionic/bulk nitrates (*i.e.*, M^+NO_3^-) with higher desorption temperature (peak at $\sim 280^\circ\text{C}$, Fig. 4A). The reaction between NO and the former species (*e.g.*, monodentate nitrate, M-O-ONO) is likely the one that gives rise to N_2O_3 (eqn (14)), whereas the reaction between NO and the latter species (NO_3^-) gives rise to ionic nitrites, NO_2^- (eqn (15)).



The rise of ionic nitrites was previously reported by Filtschew and Hess through their DRIFTS spectroscopy studies upon co-adsorbing NO and NO_2 over ceria.⁴⁴ Interestingly, they also reported that, over time, evolution of ionic nitrites is disrupted by the formation of ligated and ionic nitrates, likely due to prolonged interactions with NO_x gases in the feed. This was similarly observed by us previously where we demonstrated, through *in situ* DRIFTS analysis on the composite catalysts, the reaction of CM-derived nitrites with zeolite-stored NH_3 .³² We showed that this reaction on composite catalysts effectively titrated nitrites/nitrite intermediates from the CM surface before they could be further oxidized to nitrates with prolonged exposure to the CM surface, and only upon depletion of NH_3 stores on the zeolite are nitrate bands

observed on CM. Even in fast SCR atmosphere nitrites are still short-lived and thus their exploitation for the reaction in the zeolite component is only likely by closely coupling the oxide component to the zeolite component. This is likely why the impact of the degree of contact is still significant even under fast SCR conditions, and this also explains reduced NO_2 evolution from the impregnated CM/CSZ sample in Fig. 1A where the degree of contact is high.

It is interesting to observe that, despite the capacity of CM to catalytically decompose NH_4NO_3 as well as to generate nitrite intermediates to suppress NH_4NO_3 accumulation, stabilized NH_4NO_3 deposits still form during the fast SCR reaction over CM/HSZ and CM/CSZ. The NH_4NO_3 -TPD spectra for CM + HSZ and CM + CSZ (Fig. 7B and 8B, respectively) show that, in the temperature range of 100 – 160°C , CM begins to facilitate destabilization of NH_4NO_3 to NO_2 *via* the nitric acid intermediate. However, it is not until 200 – 300°C that the rate of catalytic decomposition of NH_4NO_3 is high and the catalytic effect becomes prominent. Therefore, at low temperature, ‘destabilized’ deposits are still expected albeit in a smaller quantity, and this is what fast-SCR-TPD data has previously demonstrated (Fig. 4C and 5B, for CM/HSZ and CM/CSZ, respectively).

Our theory of ‘destabilized’ NH_4NO_3 deposits and balanced NO + NO_2 consumption explains the remarkable NO_2 release characteristics during the temperature-programmed fast SCR reaction over the composite catalysts (Fig. 1A). We have shown that CM heavily influences both the quantity and nature of NH_4NO_3 deposits formed in the composite catalyst, and through NH_4NO_3 -TPD analysis we have also shown that CM facilitates more facile decomposition of existing NH_4NO_3 deposits. We believe that collectively these occur in a similar mechanistic fashion to CM influence on the standard SCR that we reported previously *via* the reaction of CM-derived nitrites/nitrite intermediates.³² The conventional NH_4NO_3 confinement effect likely results from hindering further reaction of the products of NH_4NO_3 dissociation (NH_3 + HNO_3) and thus stabilizing NH_4NO_3 deposits that resist dissociation and further decomposition, and acid-stabilization of NH_4NO_3 deposits likely results through similar means with additional steric or possible electrostatic influence. Thus, we believe that CM-derived nitrites react with either NH_3 or HNO_3 produced from NH_4NO_3 dissociation and thereby accelerate dissociation and further decomposition of NH_4NO_3 . Lastly, Ruggeri *et al.* reported the presence of free nitrite ions as proof of the equilibrium that exists between adsorbed nitrites and gas-phase HONO .⁴⁵ We hypothesize that this observation is at the root of CM facilitating unbound, or ‘loosely’ stored, NH_4NO_3 deposits.

Conclusions

Here we have demonstrated that composite SCR catalysts, consisting of Cu-SSZ-13 closely coupled with Ce/Mn-oxide,



exhibit reduced accumulation of NH_4NO_3 deposits and $\text{NH}_4\text{-NO}_3$ deposits that are comparatively less stable and decompose more facilely. We have shown that, in the absence of Ce/Mn-oxide, two types of NH_4NO_3 deposits form: (i) BAS-bound deposits that prevail at lower temperature form quickly at 160 °C, and are moderately stable, and (ii) Cu-bound deposits that prevail at higher temperature form slowly at 160 °C, and are more stable. In the presence of Ce/Mn-oxide, a third type of NH_4NO_3 deposit is observed that we believe is not BAS- or Cu-bound. We term these deposits ‘destabilized’ NH_4NO_3 owing to how facilely they decompose similar to physically mixed or impregnated NH_4NO_3 . Therefore, we have shown that Ce/Mn-oxide influences both the quantity and stability of NH_4NO_3 deposits formed under “fast” SCR reaction conditions. The latter is achieved by both mitigating the formation of Cu-bound NH_4NO_3 and shifting NH_4NO_3 deposits to either BAS-bound or ‘destabilized’ form that, again, are more facilely decomposed. Liu *et al.* previously showed, through IR study, reduced intensity of IR features on Cu-SSZ-13 associated with NH_4NO_3 in the presence of Mn-Ce.³⁴ However, this is, to our knowledge, the first report of the ability of SCR composite catalysts to reduce and alter the nature of NH_4NO_3 deposits formed during the SCR reaction at low temperature, and a key step in the design of SCR catalysts with low greenhouse gas impact.

We ascribe the unique influence of Ce/Mn-oxide on the total quantity and stability of NH_4NO_3 deposits to CM-derived nitrites as well as the ability of CM to balance the rate of global consumption of NO and NO_2 during the SCR reaction. We believe that this is facilitated in a similar fashion to what we reported previously which was the facile reaction of Ce/Mn-oxide-derived nitrites with NH_3 stored on the zeolite. We showed previously that: (i) at temperatures <180 °C NH_3 inhibition limits Cu involvement and Ce/Mn-oxide enhanced SCR performance solely through interaction of Ce/Mn-oxide and BAS, and (ii) at >180 °C Ce/Mn-oxide further enhanced SCR performance through interaction of Ce/Mn-oxide and Cu centers. It is directly through this influence, and as a function of temperature, that we believe stabilized NH_4NO_3 deposits are mitigated and *in situ* NH_4NO_3 decomposition is facilitated.

Author contributions

Y. W. and K. G. R. administered the project, acquired funding for the research, and supervised the work. Y. W., K. G. R., and F. G. conceptualized the research. T. A. conducted the investigation and performed analysis of data. K. G. R. and T. A. wrote the original draft of the manuscript, and K. G. R. and F. G. further reviewed and edited the manuscript.

Conflicts of interest

There are no conflicts to declare.

Acknowledgements

The authors gratefully acknowledge the U.S. Department of Energy (DOE), Energy Efficiency and Renewable Energy (EERE), Vehicle Technologies Office for the financial support of this work. PNNL is operated for the DOE by Battelle under contract number DE-AC05-76RL01830.

References

- Advanced Combustion and Emission Control Technical Road Map (https://www1.eere.energy.gov/vehiclesandfuels/pdfs/program/acec_roadmap_june2013.pdf), https://www1.eere.energy.gov/vehiclesandfuels/pdfs/program/acec_roadmap_june2013.pdf, (accessed August 20, 2019, 2019).
- F. Gao, Y. Wang, M. Kollár, N. M. Washton, J. Szanyi and C. H. F. Peden, *Catal. Today*, 2015, **258**, 347–358.
- A. Wang, Y. Wang, E. D. Walter, N. M. Washton, Y. Guo, G. Lu, C. H. Peden and F. Gao, *Catal. Today*, 2019, **320**, 91–99.
- E. Tronconi, I. Nova, C. Ciardelli, D. Chatterjee and M. Weibel, *J. Catal.*, 2007, **245**, 1–10.
- I. Nova, C. Ciardelli, E. Tronconi, D. Chatterjee and B. Bandl-Konrad, *Catal. Today*, 2006, **114**, 3–12.
- A. Grossale, I. Nova, E. Tronconi, D. Chatterjee and M. Weibel, *J. Catal.*, 2008, **256**, 312–322.
- M. Jabłońska, G. Delahay, K. Kruczała, A. Błachowski, K. A. Tarach, K. Brylewska, C. Petitto and K. Góra-Marek, *J. Phys. Chem. C*, 2016, **120**, 16831–16842.
- Y. Zha, M. Cunningham, Y. Tang, A. Srinivasan, J. Luo, J. Heichelbech, V. Lakkireddy, A. Yezerets, S. Ruffin and Z. Wei, Sustained Low Temperature NO_x Reduction, Report 0148–7191, SAE Technical Paper, 2018.
- X. Shi, F. Liu, L. Xie, W. Shan and H. He, *Environ. Sci. Technol.*, 2013, **47**, 3293–3298.
- C. Ciardelli, I. Nova, E. Tronconi, D. Chatterjee and B. Bandl-Konrad, *Chem. Commun.*, 2004, 2718–2719, DOI: **10.1039/B411613E**.
- M. Iwasaki and H. Shinjoh, *Appl. Catal., A*, 2010, **390**, 71–77.
- M. Koebel, M. Elsener and G. Madia, *Ind. Eng. Chem. Res.*, 2001, **40**, 52–59.
- A. Grossale, I. Nova and E. Tronconi, *J. Catal.*, 2009, **265**, 141–147.
- P. Forzatti, I. Nova and E. Tronconi, *Angew. Chem., Int. Ed.*, 2009, **48**, 8366–8368.
- W.-M. Chien, D. Chandra, K. H. Lau, D. L. Hildenbrand and A. M. Helmy, *J. Chem. Thermodyn.*, 2010, **42**, 846–851.
- M. V. L. Pereira, D. Berthout, C. Petitto, G. Delahay, S. Raux and S. Rousseau, *ChemCatChem*, 2017, **9**, 2339–2343.
- H.-Y. Chen, Z. Wei, M. Kollar, F. Gao, Y. Wang, J. Szanyi and C. H. F. Peden, *J. Catal.*, 2015, **329**, 490–498.
- K. R. Brower, J. C. Oxley and M. Tewari, *J. Phys. Chem.*, 1989, **93**, 4029–4033.
- A. Savara, M.-J. Li, W. M. H. Sachtler and E. Weitz, *Appl. Catal., B*, 2008, **81**, 251–257.



- 20 Y. Cui and F. Gao, *Emiss. Control Sci. Technol.*, 2019, **5**, 124–132.
- 21 F. Gao, J. Szanyi, Y. Wang, B. Schwenzer, M. Kollár and C. H. Peden, *Top. Catal.*, 2016, **59**, 882–886.
- 22 O. Mihai, C. R. Widyastuti, A. Kumar, J. Li, S. Y. Joshi, K. Kamasamudram, N. W. Currier, A. Yezerets and L. Olsson, *Catal. Lett.*, 2014, **144**, 70–80.
- 23 J. H. Kwak, D. N. Tran, S. D. Burton, J. Szanyi, J. H. Lee and C. H. F. Peden, *J. Catal.*, 2012, **287**, 203–209.
- 24 Y. Shan, X. Shi, G. He, K. Liu, Z. Yan, Y. Yu and H. He, *J. Phys. Chem. C*, 2018, **122**, 25948–25953.
- 25 Y. Shan, Y. Sun, J. Du, Y. Zhang, X. Shi, Y. Yu, W. Shan and H. He, *Appl. Catal., B*, 2020, **275**, 119105.
- 26 L. Xie, F. Liu, K. Liu, X. Shi and H. He, *Catal. Sci. Technol.*, 2014, **4**, 1104–1110.
- 27 M. Colombo, I. Nova and E. Tronconi, *Catal. Today*, 2010, **151**, 223–230.
- 28 P. S. Metkar, V. Balakotaiah and M. P. Harold, *Catal. Today*, 2012, **184**, 115–128.
- 29 N. Ottinger, Y. Xi, C. Keturakis and Z. G. Liu, *SAE Int. J. Engines*, 2017, **10**, 1646–1652.
- 30 H. Kubota, C. Liu, T. Toyao, Z. Maeno, M. Ogura, N. Nakazawa, S. Inagaki, Y. Kubota and K.-i. Shimizu, *ACS Catal.*, 2020, **10**, 2334–2344.
- 31 C. Liu, G. Malta, H. Kubota, K. Kon, T. Toyao, Z. Maeno and K.-i. Shimizu, *J. Phys. Chem. C*, 2021, **125**, 13889–13899.
- 32 T. Andana, K. G. Rappé, N. C. Nelson, F. Gao and Y. Wang, *Appl. Catal., B*, 2022, 121522, DOI: [10.1016/j.apcatb.2022.121522](https://doi.org/10.1016/j.apcatb.2022.121522).
- 33 M. Bendrich, A. Scheuer, R. E. Hayes and M. Votsmeier, *Appl. Catal., B*, 2018, **222**, 76–87.
- 34 Q. Liu, Z. Fu, L. Ma, H. Niu, C. Liu, J. Li and Z. Zhang, *Appl. Catal., A*, 2017, **547**, 146–154.
- 35 X. Wu, F. Lin, H. Xu and D. Weng, *Appl. Catal., B*, 2010, **96**, 101–109.
- 36 G. Qi and W. Li, *Catal. Today*, 2015, **258**, 205–213.
- 37 Y. Feng, T. V. W. Janssens, P. N. R. Vennestrom, J. Jansson, M. Skoglundh and H. Grönbeck, *J. Phys. Chem. C*, 2021, **125**, 4595–4601.
- 38 J. Sun, Z. Sun, Q. Wang, H. Ding, T. Wang and C. Jiang, *J. Hazard. Mater.*, 2005, **127**, 204–210.
- 39 B. J. Wood and H. Wise, *J. Chem. Phys.*, 1955, **23**, 693–696.
- 40 V. Babrauskas and D. Leggett, *Fire Mater.*, 2020, **44**, 250–268.
- 41 J. Han, A. Y. Wang, G. Isapour, H. Harelind, M. Skoglundh, D. Creaser and L. Olsson, *Ind. Eng. Chem. Res.*, 2021, **60**, 17826–17839.
- 42 Y. Z. Xi, N. A. Ottinger, C. J. Keturakis and Z. G. Liu, *Appl. Catal., B*, 2021, **294**, 120245.
- 43 S. Li, Y. Zheng, F. Gao, J. Szanyi and W. F. Schneider, *ACS Catal.*, 2017, **7**, 5087–5096.
- 44 A. Filtschew and C. Hess, *Appl. Catal., B*, 2018, **237**, 1066–1081.
- 45 M. P. Ruggeri, T. Selleri, M. Colombo, I. Nova and E. Tronconi, *J. Catal.*, 2014, **311**, 266–270.

